Molecular & Cellular Biomechanics 2024, 21(4), 1196.
https://doi.org/10.62617/mcb1196

Article

The impact of changes in nasal biomechanical properties caused by allergic rhinitis on uneven airflow distribution and exacerbation of allergic reactions

Kunrong Wang[1,2,†], Dongsheng Xing[1,3,*], Hongwei Cao[1,†], Feifei Jang[1], Aihui Yan[1,*]

[1] Department of Otorhinolaryngology, The First Hospital of China Medical University, Shenyang 110001, China
[2] Department of Otorhinolaryngology, The Third People's Hospital of Dalian, Dalian 116033, China
[3] Department of Otorhinolaryngology, Liaoyang Central Hospital, Liaoyang 111000, China
*** Corresponding authors:** Aihui Yan, ymxs163163@163.com; Dongsheng Xing, dsxing1987@126.com
[†] Kunrong Wang and Hongwei Cao contributed to this work equally

CITATION

Wang K, Xing D, Cao H, et al. The impact of changes in nasal biomechanical properties caused by allergic rhinitis on uneven airflow distribution and exacerbation of allergic reactions. Molecular & Cellular Biomechanics. 2024; 21(4): 1196. https://doi.org/10.62617/mcb1196

ARTICLE INFO

Received: 19 November 2024
Accepted: 24 December 2024
Available online: 31 December 2024

Abstract: Allergic rhinitis (AR) is a common chronic condition characterized by an exaggerated nasal response to allergens, significantly impacting airflow and exacerbating symptoms. Structural changes in the nasal cavity, such as septal deviation and turbinate hypertrophy, disrupt normal airflow dynamics, prolonging allergen retention and intensifying inflammation. The interplay between anatomical abnormalities, increased inflammatory mediators, and biomechanical feedback mechanisms creates a cycle that amplifies AR symptoms. **Methods:** Based on the results of thin-layer CT scans of the nasal cavity for 20 patients with nasal septum deviation and 20 healthy northern Chinese individuals, a three-dimensional reconstruction was performed using surface reconstruction finite element partitioning methods to simulate the airflow characteristics through the nasal airways. **Results:** In individuals with nasal septum deviation, the bilateral nasal airflow distribution is primarily on the side with the wider airway, with the maximum airflow concentrated in the middle part of the total nasal passage on the wider side; the nasal airway pressure drops most rapidly at the site of greatest deviation, accounting for 79.65% of the total pressure difference across the airway. In healthy individuals, the bilateral nasal airflow is influenced by the nasal cycle, predominantly occurring on one side, with the maximum airflow distributed in the middle and lower parts of the total nasal passage; the nasal airway pressure drops most rapidly at the nasal threshold, accounting for approximately 58.78% of the total pressure difference across the airway. **Conclusion:** Using computer simulation to establish a numerical model of the nasal structure and analyze the relationship between anatomical abnormalities and airflow field characteristics represents a feasible scientific approach for studying the correlation between nasal structure, function, and disease. This can provide references for surgical treatment plans aimed at optimizing airflow paths and altering airflow distribution, as well as for personalized assessments before and after surgery. These biomechanical changes are crucial for developing targeted surgical and medical treatments, enabling more accurate disease assessment and personalized treatment plans. This knowledge also inspires the development of innovative therapies, improves symptom control, and offers hope for more effective AR management in the future.

Keywords: nasal septum deviation; three-dimensional reconstruction; numerical model; nasal cavity structural abnormalities

1. Introduction

The nasal cavity plays a crucial role in conditioning the air we breathe, ensuring it is humidified, warmed, and filtered before reaching the lungs. Allergic Rhinitis (AR) disrupts this delicate balance by causing inflammation and structural changes within

the nasal cavity. When exposed to allergens, individuals with AR experience an exaggerated immune response, leading to symptoms such as sneezing, runny nose, and congestion. Over time, chronic inflammation can cause the nasal septum to deviate and the turbinates to become hypertrophied or enlarged. These structural alterations impede normal airflow, creating areas where allergens can become trapped, prolonging their contact with the nasal mucosa and intensifying the allergic reaction.The altered biomechanics of the nasal cavity in AR patients lead to abnormal airflow patterns, which further exacerbates symptoms. Dysregulated airflow can result in increased turbulence and decreased filtration efficiency, allowing more allergens to reach deeper parts of the respiratory tract. Additionally, impaired mucus drainage can contribute to sinusitis and other complications. Studies by Ding et al. [1], Sajjadi et al. [2], and Andersen et al. [3] have found that exercising in polluted environments may not necessarily benefit health; Kuehn [4] has pointed out that walking in clean environments significantly improves lung function and other aspects of health; there is a necessity to quantify the risks associated with various pollutants to human health to improve population health [5]. Therefore, the issue of harmful particle deposition in respiratory airflow is closely related to healthy and effective exercise. This study employs this method to investigate the mechanisms and influencing factors of particle deposition in the human nasal and nasopharyngeal cavities, providing references for optimizing intranasal drug administration methods and improving medication efficiency in clinical settings.

2. Materials and methods

2.1. Materials

Nasal Septal Deviation Group (Experimental Group): Twenty patients with nasal septal deviation accompanied by varying degrees of symptoms such as nasal congestion, headaches, and nosebleeds were selected. The age range was between 20 to 60 years old, including 14 males and 6 females, all from the northern region. The medical history ranged from 10 to 20 years, with an average of 16.7 years. Nasal endoscopy and anterior rhinoscopy examination showed a “C”-shaped deviation of the nasal septum (which may include compensatory changes in one or both turbinates), and cases with nasal polyps or other nasal diseases were excluded. Healthy Control Group: The healthy control group consisted of 20 healthy individuals aged 20–60 years from the northern region who, after detailed medical history inquiry, were confirmed to have no history of chronic upper respiratory disease, no history of nasal trauma or surgery, and no history of acute upper respiratory infection in the last 3–6 months. Prenasal rhinoscopy and nasal endoscopy showed no signs of otolaryngology disease or significant anatomic abnormalities. Philips 128-slice multi-row spiral CT scanner; Dell-Precision Tower 7810 desktop workstation, motherboard chipset: Intel C612, CPU model: Xeon E5-2609V3, graphics card chip: nVIDIA Quadro, standard CPU core count: 12; Mimics 15.0 image processing software; Geomagic 17.0 reverse engineering software; ANSYS 15.0 finite element analysis software.

2.2. Methods

2.2.1. Multi-slice spiral CT scan

The selection of multi-slice spiral CT scan parameters is crucial for accurately assessing nasal structures and airflow patterns, especially in patients with Allergic Rhinitis (AR). Layer thickness, window width, and window level settings play significant roles in the detailed display of nasal anatomy and the accurate identification of airway boundaries. Thicker slices may reduce image noise but can miss small anatomical details, making it challenging to evaluate fine structures like the turbinates and septum, which are essential in AR patients for assessing airway obstructions. Conversely, thinner slices provide higher spatial resolution, allowing for better visualization of these critical structures. For instance, a slice thickness of 0.625 mm or 1.25 mm can reveal intricate details such as minor deviations in the nasal septum or subtle mucosal thickening on the turbinates, which are often overlooked with thicker slices. Window width and window level adjustments optimize contrast between different tissues, enhancing the visibility of bone structures and soft tissues. Proper settings ensure that the nasal airway boundaries are clearly delineated, which is vital for accurate measurement and assessment.

A typical bone window setting might use a width of around 2000 HU and a level of about 300 HU to clearly display the bony anatomy, while a soft tissue window with a width of approximately 400 HU and a level of 40 HU is more suitable for observing the soft tissue structures within the nasal passages. These precise imaging details are fundamental for constructing accurate computational models used in simulations to predict airflow dynamics and the impact of anatomical changes on respiratory function. By ensuring these parameters are optimized, healthcare providers can improve diagnostic accuracy and treatment planning, ultimately enhancing patient outcomes through more personalized and effective care strategies.Subjects underwent nasal continuous scanning using a spiral CT (Siemens, Germany, model: Somatom Emotion 16) from the tip of the nose to the posterior wall of the nasopharynx, with a slice thickness of 3 mm and soft tissue window (window width 2000, window level 400). The choice of a 3-mm slice thickness for nasal continuous scanning is based on several factors. Firstly, it allows for a balance between capturing detailed anatomical structures and maintaining acceptable scan times. A thinner slice thickness would provide higher spatial resolution, which is beneficial for discerning fine details such as mucosal layers and blood vessels. However, thinner slices require more data and thus longer scan times, which may not be feasible or desirable in clinical settings. On the other hand, a thicker slice thickness reduces the amount of data acquired and speeds up the scan process. This is particularly useful for areas such as the nasal cavity, where the anatomy is relatively simple and the spatial resolution requirements are not as stringent as in other areas such as the brain or spinal cord.In addition, the choice of a 3-mm slice thickness is often guided by the specific clinical question or indication being addressed. For example, if the goal is to evaluate sinusitis or structural abnormalities, a thicker slice may be sufficient to visualize the overall extent of the disease or abnormality. In contrast, if the goal is to assess subtle mucosal changes or blood flow，a thinner slice may be required.

The obtained DICOM imaging data were converted into BMP format images using software provided by the CT machine. The volunteer's nasal and nasopharyngeal regions were scanned using multi-slice spiral CT, and the obtained DICOM format image data was imported into MIMICS 15.0 to establish a numerical model of the upper airway. The continuous coronal CT images of nasal septum deviation are shown in **Figure 1**. The continuous coronal CT images of a healthy nasal cavity are shown in **Figure 2**. The model was then processed using Geomagic 17.0 software to obtain a complete three-dimensional model with smooth surfaces. Subsequently, Ansys 15.0 ICEM platform was used for mesh reconstruction, setting the entrance of the airway model at both anterior nares and the exit at the plane below the glottis. The model was then divided into meshes, and the processed model was imported into the Fluent platform in .mes format for numerical simulation. The grid count was 2.46×10^6, and the node count was 4.3×10^5. Various boundary conditions and variable settings were applied to the obtained model: Particle diameters (d) of 5, 10, and 15 μm; particle densities (ρ) of 1250, 1850, and 2150 kg/m^3; and airflow rates (Q) of 15, 30, and 60 L/min. The particle phase was set under the following conditions: No interaction between particles, their motion does not affect the airflow field; particles in the flow field are influenced by gravity, Saffman lift force, and pressure gradient force; particles in the airway are either "captured" or "escaped", without evaporation or fragmentation; particles are spherical coal dust particles of the same diameter.

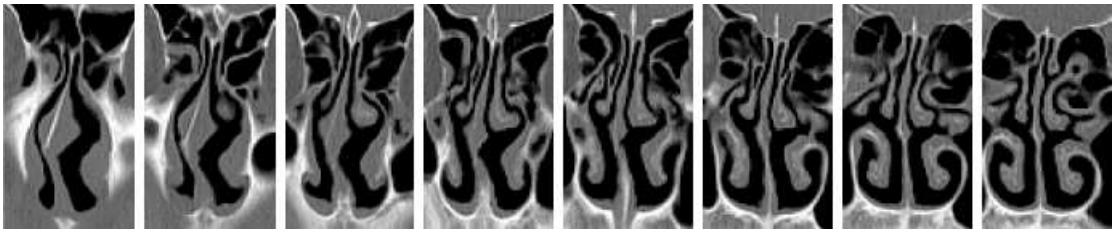

Figure 1. The continuous coronal CT image of nasal septum deviation.

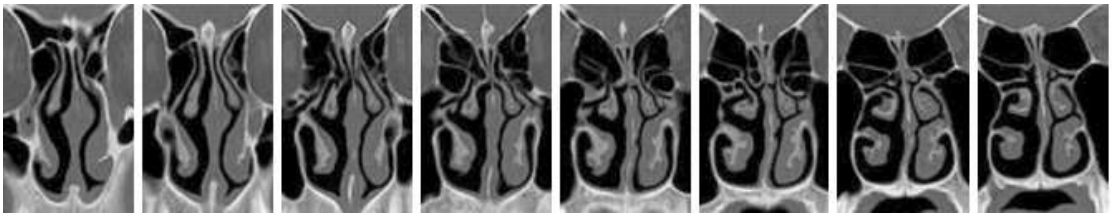

Figure 2. The continuous coronal CT image of healthy nasal cavity.

2.2.2. Three-dimensional reconstruction: The BMP format images obtained were digitized using Matlab software

A custom-compiled program was used to identify the boundaries of the nasal airway, which were then imported into Ansys 10.0 software. Using the preprocessing functions of this software, key points that reflect the structural features of the airway on each layer were manually selected and connected to form lines. These lines were further used to construct surfaces and volumes. Tetrahedral elements were chosen to perform a finite element mesh on the volume for surface three-dimensional reconstruction of the nasal airflow passage.

2.2.3. Calculation of airflow field: The Ansys10.0 post-processing function was used in conjunction with the Navier-Stokes equations for viscous fluid motion to calculate the nasal airflow field

The boundary conditions were set as follows: (1) No-slip boundary condition at the nasal airway walls, i.e., Vs = 0 m/s; (2) One standard atmospheric pressure at the nostrils (p = 101,325 Pa); (3) The airflow velocity at the nasopharynx (m/s) was determined based on the range of respiratory frequency and tidal volume under physiological conditions of Chinese individuals. A respiratory cycle (T) of 3 s was selected, with a tidal volume of 500 mL, equivalent to a ventilation rate of 10 L/min. Assuming equal breathing time, the breathing process was modeled as a sinusoidal variation pattern. The area of the nasopharyngeal airway was calculated by the model, and then the average airflow velocity at the nasophararynx was determined by measuring the respiratory volume. The selection of particle size typically depends on the objectives and practical applications of the research. Different density values can be used to simulate various types of particles, and the choice of airflow rate determines the transmission speed and residence time of the particles in the system.

Based on the three-dimensional reconstruction model, the cross-sectional area of the nasopharynx, the pressure difference between the anterior and posterior parts of the nasal cavity, and the airflow rate at the nasopharynx were obtained. The nasal resistance was calculated using the formula [6]: Nasal resistance = pressure difference between the anterior and posterior parts of the nasal cavity/gas flow rate. Additionally, we used a nasal resistance meter to measure the nasal resistance in the subjects mentioned above.

2.3. Statistical analysis

Statistical analysis software SPSS 12.0 was used to perform statistical analysis on the airflow distribution at different parts of the nasal airway in both the experimental group and the control group. The experimental data are expressed as mean ± standard deviation ($x \pm s$). A two-sample t-test was used for bilateral corresponding positions. Differences were considered statistically significant at $p < 0.05$.

3. Results

3.1. Airflow velocity and airway area distribution

The airflow velocity distribution cloud map for individuals with a deviated nasal septum is shown in **Figure 3**. The airflow velocity on the side with the wider airway is faster compared to the side with the narrower airway; the cross-sectional area on the side of the nasal airway that is more spacious is larger. Both are most pronounced in the middle of the total nasal passage, as seen in **Table 1**.

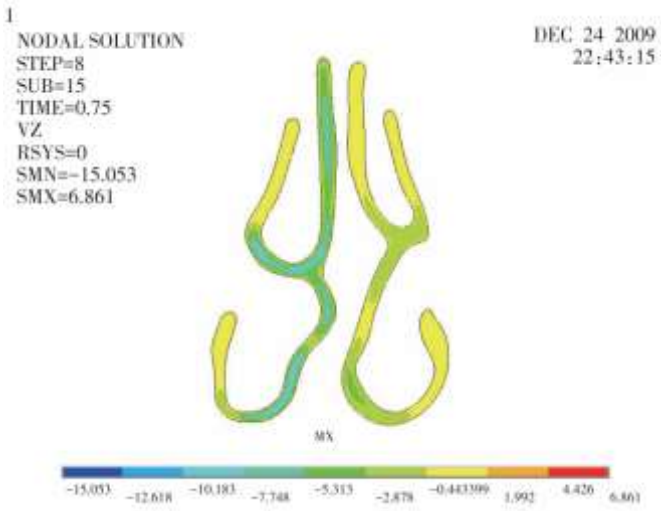

Figure 3. The airflow distribution in patients with nasal septum de-viation.

Table 1. Comparison of airflow volume, airflow velocity, and airway area at corresponding positions in the nasal airway of both sides for the experimental group.

Detected part	Fluence ($\times 10^{-4}$ m^3/s)			Airflow rate (m/s)			Area of airway ($\times 10^{-4}$ $m^{2)}$		
	Wide side	**Narrow side**	***t***	**Wide side**	**Narrow side**	***t***	**Wide side**	**Narrow side**	***t***
Meatus nasi communis	2.98 ± 0.57	1.10 ± 0.65	4.782[1)]				2.97 ± 0.22	1.03 ± 0.67	2.832[1)]
Middle of meatus nasi communis	1.04 ± 0.42	0.19 ± 0.17	4.644[1)]	3.01 ± 1.94	0.30 ± 0.13	2.724[1)]	1.02 ± 0.44	0.18 ± 0.13	2.671[1)]
Inferior part of meatus nasi communis	0.80 ± 0.48	0.59 ± 0.50	0.680	1.93 ± 1.02	1.53 ± 1.00	0.757	0.41 ± 0.27	0.15 ± 0.09	0.312
Middle nasal meatus	0.71 ± 0.29	0.20 ± 0.01	0.979	1.67 ± 1.34	0.75 ± 0.23	1.639	0.35 ± 0.20	0.14 ± 0.07	1.459
Inferior nasal meatus	0.35 ± 0.25	0.19 ± 0.07	1.364	1.29 ± 0.97	0.42 ± 0.32	1.042	0.49 ± 0.24	0.48 ± 0.17	0.158
Olfactory cleft	0.18 ± 0.13	0.12 ± 0.09	0.421	0.39 ± 0.21	0.17 ± 0.02	0.132	0.25 ± 0.19	0.21 ± 0.08	0.305

1) $p < 0.05$.

The airflow velocity distribution cloud map for the bilateral nasal passages of healthy individuals is shown in **Figure 4**. Influenced by the nasal cycle, among the 20 subjects, 16 (80%) primarily ventilated through one side of the nasal cavity. The airflow velocity was faster on the main ventilation side compared to the non-main ventilation side, particularly in the middle and lower parts of the total nasal passage. There was no statistically significant difference in the cross-sectional area of the nasal airway between both sides ($p > 0.05$). See **Table 2**.

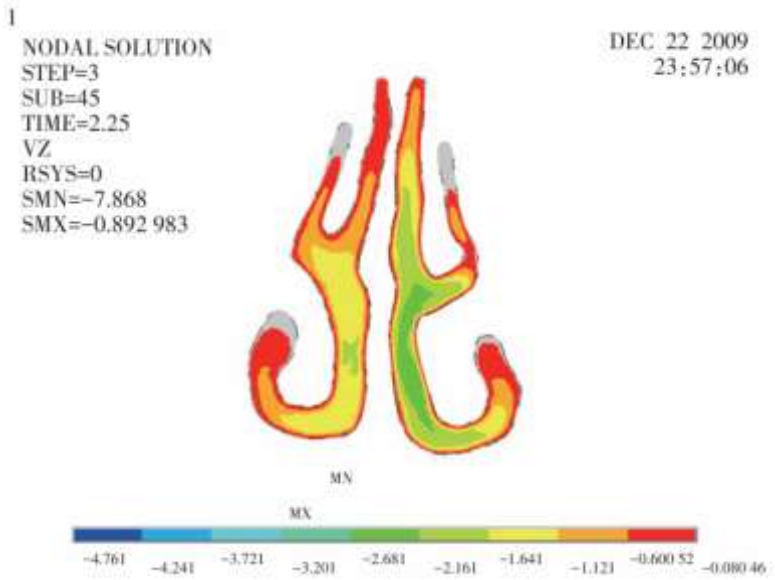

Figure 4. The airflow distribution of healthy nasal cavity.

Table 2. Thecomparison of fluence, airflowr ate, area of airway of two air passage in the control group.

Detected part	Fluence (× 10^{-4} m^3/s)			Airflow rate (m/s)			Area of airway (× 10^{-4} $m^{2)}$		
	Main venting side	Secondary venting side	*t*	Main venting side	Secondary venting side	*t*	Main venting side	Secondary venting side	*t*
Meatus nasi communis	4.05 ± 0.80	2.46 ± 0.56	4.293[1)]				2.25 ± 0.39	2.05 ± 0.36	0.986
Middle of meatus nasi communis	1.68 ± 0.34	0.73 ± 0.33	2.539[1)]	3.18 ± 0.89	2.08 ± 0.85	2.647[1)]	0.61 ± 0.06	0.56 ± 0.07	1.558
Inferior part of meatus nasi communis	0.84 ± 0.38	0.44 ± 0.24	2.368[1)]	2.33 ± 1.24	1.20 ± 0.43	2.275[1)]	0.40 ± 0.09	0.33 ± 0.08	1.708
Middle nasal meatus	0.80 ± 0.32	0.79 ± 0.28	1.429	2.19 ± 1.07	1.05 ± 0.50	1.376	0.42 ± 0.10	0.41 ± 0.09	0.326
Inferior nasal meatus	0.40 ± 0.27	0.28 ± 0.16	1.097	1.14 ± 0.49	0.78 ± 0.54	0.669	0.52 ± 0.30	0.47 ± 0.25	0.326
Olfactory cleft	0.33 ± 0.14	0.18 ± 0.13	1.065	1.02 ± 0.03	0.67 ± 0.50	1.666	0.29 ± 0.04	0.28 ± 0.04	0.310

1) $p < 0.05$.

3.2. Nasal airway pressure distribution

The nasal airway pressure in both groups of subjects gradually decreased from the nostrils to the nasopharynx. In the experimental group, the most significant drop in pressure occurred at the site of the most pronounced deviation of the nasal septum on the narrower side (i.e., the narrowest part of the nasal airway) (**Figure 5**), accounting for approximately 79.65% of the total pressure difference in the airway. The range of pressure difference from the nostrils to the nasopharynx was (248 ± 12) Pa. In the control group, the fastest drop in pressure occurred near the nasal valve (**Figure 6**), accounting for about 58.78% of the total pressure difference in the airway. The range of pressure difference from the nostrils to the nasopharynx was (131 ± 91) Pa.

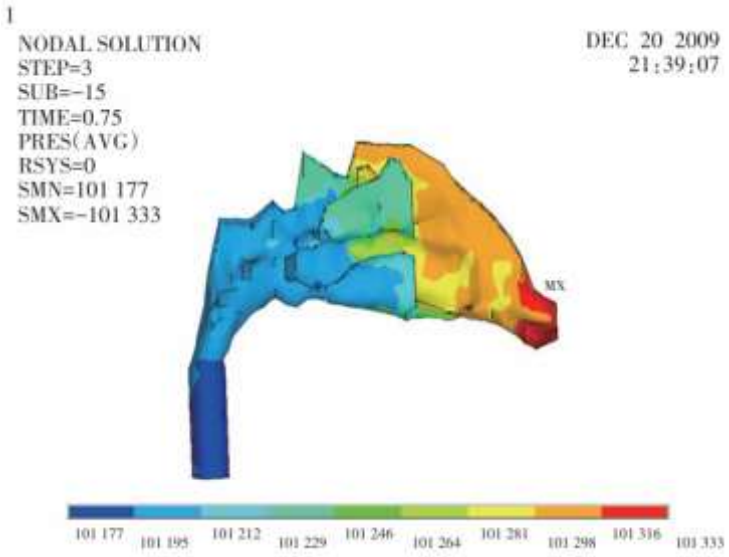

Figure 5. The nasal cavity pressure of nasal septum deviation.

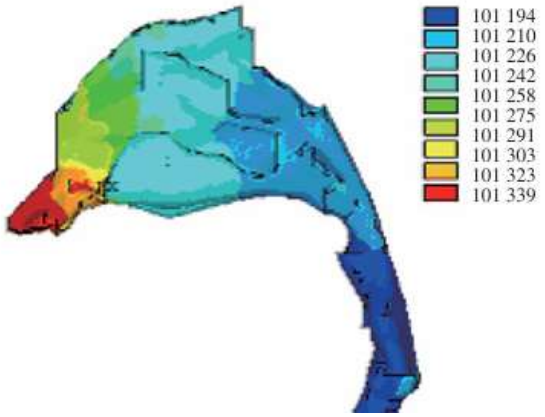

Figure 6. The nasal cavity pressure of healthy nasal cavity.

3.3. Nasal resistance measurement

According to the data calculated from the reconstruction model, the nasal airway resistance for the experimental group was (0.488 ± 0.27) kPa/(L s), and for the control group it was (0.164 ± 0.03) kPa/(L s). The difference between the two groups was statistically significant (t = 2.382, p < 0.05). Using a nasal resistance meter, the nasal airway resistance for the experimental group was measured to be (0.479 ± 0.09) kPa/(L s), and for the control group it was (0.175 ± 0.11) kPa/(L s). The difference between the two was also statistically significant (t = 2.327, p < 0.05).

Generally speaking, the particle deposition rate on the posterior wall of the nasopharyngeal roof decreases as the particle diameter increases. Only when the particle density is 1250 kg/m^3 and the airflow rate is 15 L/min does the deposition rate increase with increasing particle diameter (5–10 μm) (**Figure 7**).

The general trend of particle deposition on the posterior wall of the nasopharyngeal roof with different particle diameters and densities varies with airflow rate: It decreases as the airflow rate increases. Only for a particle diameter of 5 μm

and densities of 1250, 1850, and 2150 kg/m^3 does the deposition rate increase with the airflow rate (15–30 L/min) (**Figure 8**).

Under different particle diameters and airflow rates, the deposition pattern of particles on the posterior wall of the nasopharyngeal roof with varying density follows this rule: When the particle diameter and airflow rate remain constant, the deposition rate tends to stabilize as the density increases (**Figure 9**).

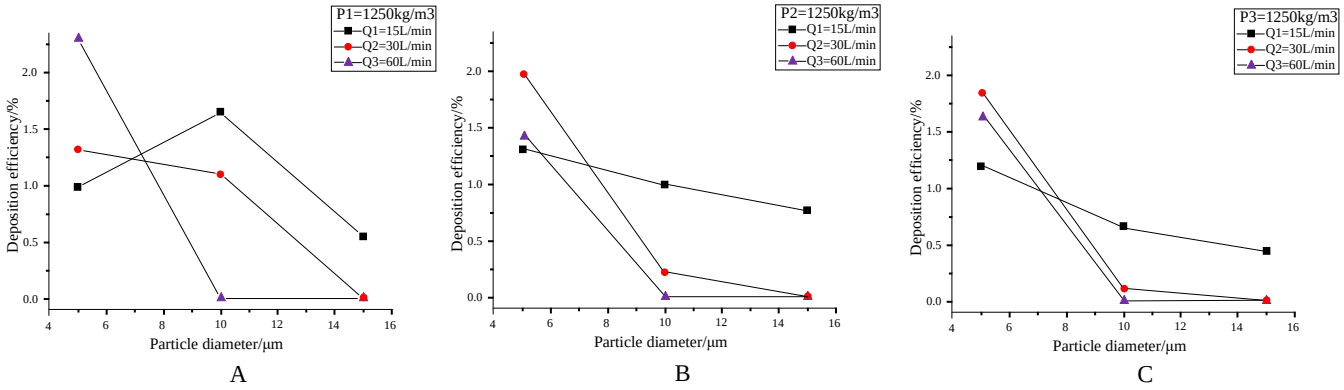

Figure 7. Shows the variation in particle deposition rate on the posterior wall of the nasopharynx. The deposition rates change with particle diameter when the flow rates (Q) are set at 15, 30, and 60 L/min, and the particle densities (ρ) are 1250, 1850, and 2150 kg/m^3 respectively (labeled as A, B, C).

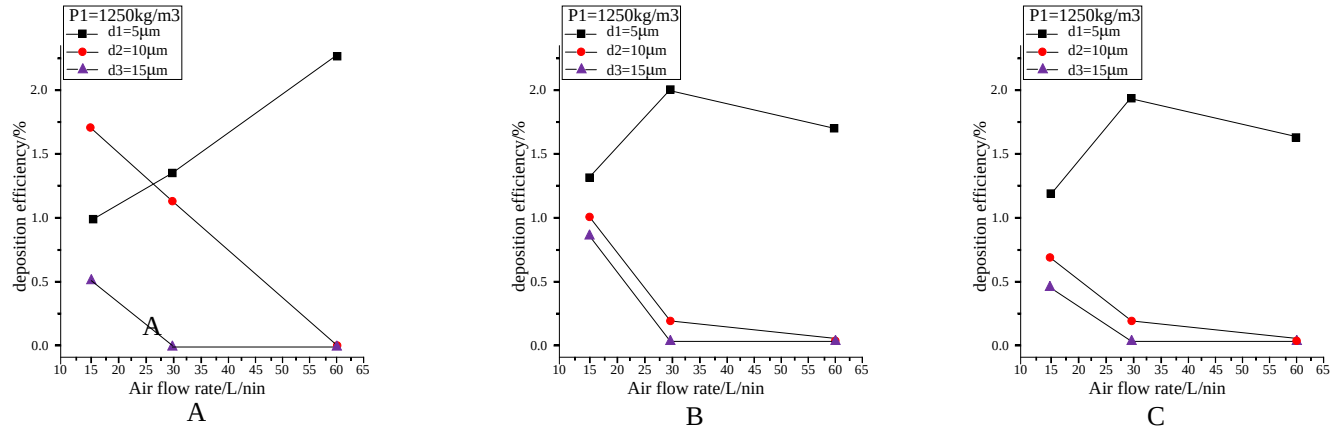

Figure 8. Shows the variation in particle deposition rate on the posterior wall of the nasopharynx. The deposition rates change with airflow rate when the particle diameters (d) are set at 5, 10, and 15 μm, and the particle densities (ρ) are 1250, 1850, and 2150 kg/m^3 respectively (labeled as A, B, C).

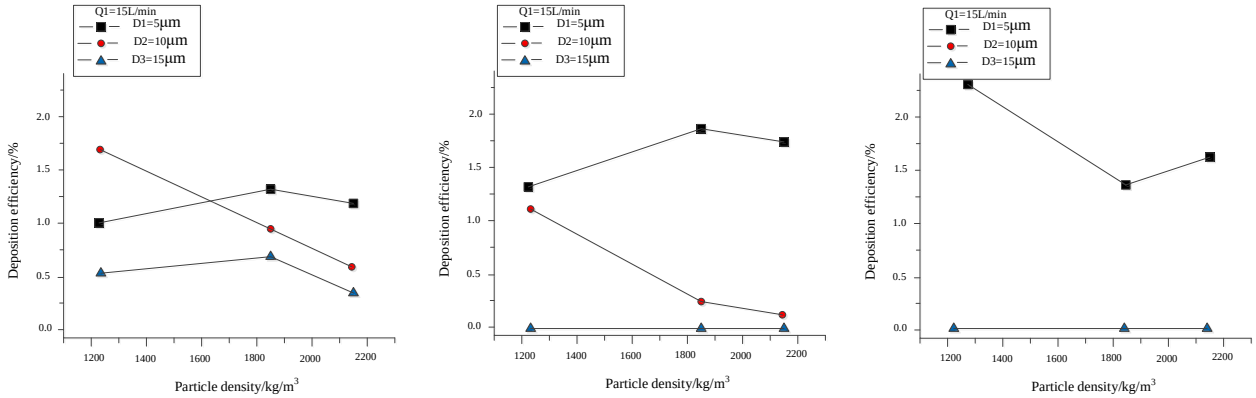

Figure 9. Shows the variation in particle deposition rate on the posterior wall of the nasopharynx. The deposition rates change with particle density when the particle diameters (d) are set at 5, 10, and 15 μm, and the airflow rates (Q) are 15, 30, and 60 L/min respectively (labeled as A, B, C).

4. Discussion

The nasal septum deviates from the midline, causing narrowing of one or both sides of the nasal cavity. This structural abnormality affects the normal ventilation function of the nasal cavity and increases the risk of sinusitis. The incidence of sinusitis is higher in patients with a deviated nasal septum. Through endoscopic examination, the position and shape of the nasal septum can be observed directly, and combined with CT scans and other imaging techniques, the deviation of the nasal septum and its associated sinusitis can be accurately diagnosed. There is a close relationship between the deviated nasal septum and sinusitis, and surgical treatment can effectively improve the patient's olfactory function, providing more evidence for clinical decision-making. The complex and intricate structure of the human upper respiratory tract increases the difficulty of studying particle deposition in this region. With the continuous development of computer technology, many institutions both domestically and internationally have conducted in-depth explorations of particle deposition in the upper respiratory tract through numerical simulations and other methods. Deng et al. [7] established a model based on detailed mathematical descriptions of airway bifurcation geometry; Yu et al. [8] utilized CT data of the respiratory tract to reconstruct a numerical model and simulate the characteristics of particle deposition within the respiratory tract, finding that particles are highly likely to deposit at positions where the airway geometry is complex or experiences significant directional changes. Farnoud et al. [9] simulated nasal aerosol particle diffusion and deposition under constant inhalation flow rates of 4.78 L/min and 7.5 L/min with monodisperse particles of diameters 2.4 μm and 10 μm. Burgos et al. [10] used computational fluid dynamics (CFD) methods to find possible links between changes in nasal airflow and the etiology of chronic suppurative otitis media. Mohamadi and Fazeli [11] applied CFD methods to study COVID-19, discovering that maintaining social distance and wearing masks could reduce the spread of virus-laden droplets. Gupta et al. [12] used CFD models to predict the spread of respiratory droplets among passengers in airplane cabins, finding that coughing significantly increased the number of inhaled droplets, and proposed that wearing N95 respirators could greatly reduce the risk of virus transmission [13]. Abuhegazy et al. [14] also

applied CFD to study how ventilation affects the spread of respiratory droplets in simulated operating rooms and restaurants.

To validate the authenticity of CFD simulation results, researchers combined CFD with in vitro experiments using 3D replicas: Kelly et al. [15], Cheng et al. [16], and Wen et al. [17] used airway 3D models to verify particle deposition; Zhou et al. [18] conducted in vitro experiments and CFD analysis on nasal replicas for particle deposition; Schroeter et al. [19] compared CFD predictions with experimental measurements; all found high agreement and similar trends between total deposit amounts obtained from in vitro experiments and CFD predictions.

In this study, we established a three-dimensional numerical model based on CT imaging and applied the CFD method to conduct experiments simulating the real human upper airway environment. During the research process, we compared the deposition efficiency (DE) with the inertial parameter, $da^2 \times Q$ ($\mu m^2 \cdot cm^3/s$), where Q and da represent the inhalation flow rate and particle diameter, respectively (**Figure 10**). We found that our simulation results were similar to the early studies by Kelly et al. [20] and Calmet et al. [21] in terms of inertial parameters. Deposition efficiency = total number of particles deposited in the target area/total number of released particles.

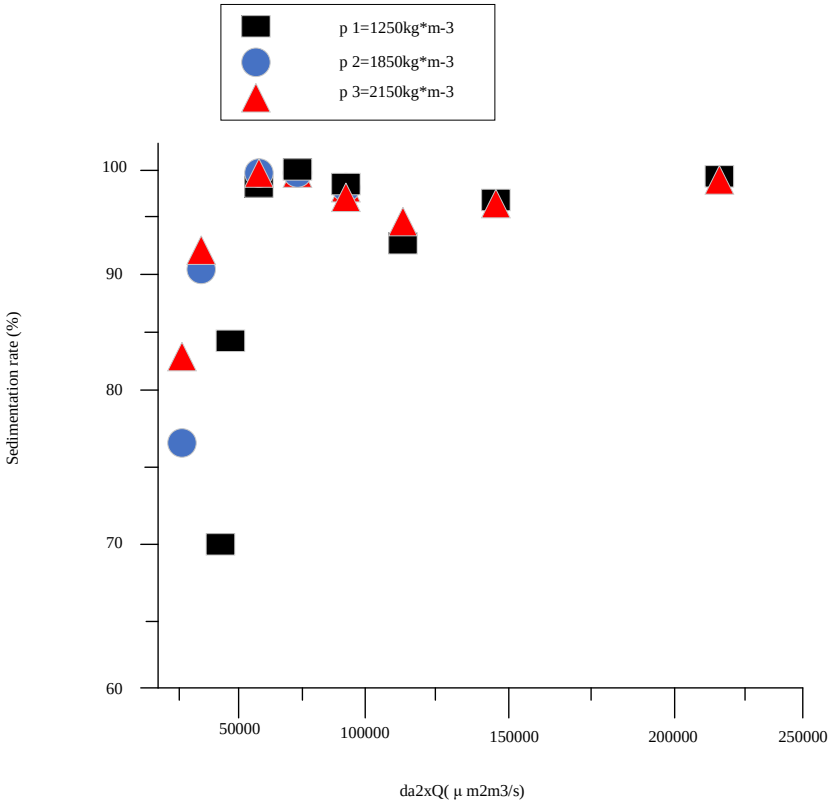

Figure 10. The variation of the deposition rate with inertial parameters. da is the particle diameter, and Q is the airflow rate.

We observed that as the breathing flow rate increased, particles were more likely to settle in the anterior part of the nasal cavity; during calm breathing, more particles settled in the nasopharynx, with more escaping from the throat. Regarding the impact of airflow rate on particle deposition, Jin et al. [22] and Koullapis et al. [23] found that an increase in airflow rate would increase inertial collisions, thereby increasing

deposition efficiency; Ahookhosh et al. [24] chose flow rates of 30, 60, 90, and 120 L/min and confirmed that an increase in flow rate would raise deposition efficiency; Sosnowski et al. [25] verified that under no-flow conditions, inertia causes droplets to mainly deposit in the front part of the nasal cavity, and then secondary diffusion occurs as patients inhale, leading to the transport of droplets deeper into the nasal cavity. Based on the simulation results of this study, we believe that in dusty air short breathing cycles (such as during intense exercise) often increase the risk of inhalation of distal lungs and bronchi, while calm breathing is more favorable for nasal spray or intranasal drug aerosol inhalation therapy for nasal diseases.

Our choice of particle diameters was based on the consideration that particles < 2.5 μm are easily suspended and not easily settled, while larger particles are often blocked by the nasal hair in the vestibule and do not easily enter the nasal cavity. The study found that when airflow rate and particle density remain constant, as particle diameter increases, the overall deposition rate in the model increases; for small particle diameters, as airflow rate increases, the deposition rate in the nasophararynx increases, whereas for large particle diameters, as airflow rate increases, their deposition rate in the nasophararynx decreases instead. This situation is considered due to large particles being easily collided and settled at positions such as the nasal threshold and turbinates, making it difficult for them to enter the nasophararynx. Regarding the relationship between particle diameter and deposition rate, some scholars have pointed out that when the drug particle diameter exceeds 10 μm, giving a smaller tidal volume results in higher deposition in the turbinate region, whereas when the drug particle diameter is less than 5 μm, a higher tidal volume is needed to increase deposition in the turbinate region [26]; Kiaee et al. [27] found that spray particle passage through the upper airway is insensitive to release velocity but highly sensitive to particle size; Calmet et al. [28] explored the relationship between sniffing, constant flow, and breath-holding breathing rates with nasal spray administration, finding that compared to breathing rate, drug particle size has the greatest impact on its deposition rate, thus proposing that selecting the appropriate particle size is crucial for drug distribution when choosing an intranasal administration strategy.

All these further illustrate that the relationship between particle diameter and airflow rate on particle deposition should not be a single one, with particle diameter having the primary influence. Our study also concluded that particle diameter, airflow speed, and particle density all affect particle deposition, with particle diameter having the greatest influence, followed by airflow rate, and density having a negligible effect on deposition rate; when particle density and airflow rate are constant, compared to 10 μm and 15 μm particles, those with a diameter of 5 μm settle the most in the nasopharynx.

The various structures of the upper airway are closely related to their functions. The primary functions of the nasal cavity include warming and humidifying inhaled air, filtering dust, and olfactory sensations. Abnormalities in nasal structure are mainly manifested in the nasal septum and inferior turbinate. The degree of deviation of the nasal septum and the size of the inferior turbinate determine the cross-sectional area of the effective airflow pathway in the nasal cavity. Studying the biomechanical numerical model of the human nasal cavity and sinuses aims to investigate the relationship between the anatomical structure of the upper airway and related diseases

from a biomechanical perspective, thereby serving clinical needs. To verify the reliability of the computer numerical model, during the experimental process, we validated the nasal resistance data calculated based on the numerical model for all subjects using a nasal resistance meter. Both methods showed that the nasal resistance in the experimental group was higher than in the control group, and there was no statistically significant difference in nasal resistance measured by the two methods ($p > 0.05$). Therefore, it can be concluded that the numerical model established in this study essentially reflects the characteristics of the nasal airways in individuals with abnormal nasal structures and in healthy people.

The numerical simulation of the upper airway nasal airflow field in healthy individuals in this experiment is consistent with the characteristics of the nasal airflow field in normal Chinese individuals studied by Sun Xiuzhen et al. The study also found that both individuals with a deviated nasal septum and healthy individuals are affected by the nasal cycle during respiration. However, compared to the nasal cycle, anatomical abnormalities of the nasal cavity have a more significant impact on the distribution of airflow passing through the nasal cavity. Individuals with a deviated nasal septum have asymmetrical nasal cavity volumes, and during respiration, the airflow volume through the narrower side of the nasal passage is significantly reduced, especially in the middle part of the total nasal passage on that side. As the airflow volume decreases, the airflow velocity also slows down, affecting the normal drainage function of the sinus openings in the middle nasal passage on that side, thereby leading to the occurrence of sinusitis on that side. To increase the airflow volume, the inferior turbinate on that side often undergoes varying degrees of atrophy and becomes smaller, manifesting as thinning of the mucosa, bone resorption, and lateral displacement, thereby reducing the resistance of the nasal airway on that side. We believe this is an adaptive change in the human nasal cavity. On the side with a wider airway, due to the long-term chronic impact of larger airflows, compensatory hyperplasia occurs in the nasal tissues on that side, and the degree and extent of lesions in the middle nasal passage mucosa may even exceed those on the opposite side, similarly leading to an increased incidence of sinusitis on that side. Moreover, our study found that individuals with high-position deviations of as opposed to low-position deviations, have a greater difference in airflow volume and velocity in the middle part of the total nasal passage on both sides at the site of the most pronounced deviation. This finding may be one of the reasons why scholars have mentioned that individuals with high-position deviations have a higher incidence of sinusitis.

The study of nasal airflow field characteristics can also be applied to the etiological analysis of olfactory changes in patients. In individuals with a deviated nasal septum, the airflow volume decreases and the airflow velocity slows down on the narrower side of the airway, and due to the diversion effect of the narrow airway, local turbulence increases. Additionally, due to the anatomical characteristics of the olfactory cleft itself, the airflow entering this area is reduced even more significantly. Based on the studies by Zhang et al. [7]. on the transport and deposition of microparticles in the upper airway model, as well as Zeng and Zhu [27]. who investigated the relationship between particle deposition rates and airflow velocities and particle inertia sizes through gas dynamic models, we have reason to believe that as the distribution of airflow entering the olfactory cleft area on the affected side

changes, the particles causing olfaction that enter and deposit in the olfactory area are significantly reduced or even absent, leading to a reduction or loss of smell.

Therefore, we believe that numerical simulation of pathological upper airway structures and the analysis of the relationship between anatomical abnormalities and airflow field characteristics can be used to evaluate the causal mechanisms between upper airway structure-function-disease interactions. This, in turn, provides a reference for surgical treatments aimed at optimizing airflow paths and altering airflow distribution.

Author contributions: Conceptualization, KW, DX and AY; methodology, KW; software, DX validation, KW, DX and AY; formal analysis, HC; investigation, FJ; resources, XX; data curation, XX; writing—original draft preparation, XX; writing—review and editing, KW; visualization, KW; supervision, DX; project administration, AY; funding acquisition, AY. All authors have read and agreed to the published version of the manuscript.

Ethical approval: The study was conducted in accordance with the Declaration of Helsinki, and approved by the Ethics Committee of The First Hospital of China Medical University. Approval number is 2024011101. The date of approval is 2024.1.11. All participants signed the informed consent in this study.

Conflict of interest: The authors declare no conflict of interest.

References

1. Kotova E N, Bogomilsky M R,Sidorenko E I and Baranov K K.(2021).[Features of the architectonics of the structures of the nasal cavity and choanal zone in children with congenital malformations of the eyes]..Vestnik otorinolaringologii(1),63–67.
2. Laura Cristina Oyarzun, Hartwig Katrin, Distergoft Alexander, Hoffmann Tim, Scheckenbach Kathrin,Bruesseler Melanie and Wesarg Stefan.(2021).Automatic segmentation of the structures in the nasal cavity and the ethmoidal sinus for the quantification of nasal septal deviations.MEDICAL IMAGING 2021: COMPUTER-AIDED DIAGNOSIS
3. Markeeva M. V., Aleshkina O. Yu.,Tarasova N. V. and Gaivoronsky I. V..(2020).Anatomycal features of the ethmoidal labyrinth and nasal cavity structures in childhood.Bulletin of the Russian Military Medical Academy(4),95–99.
4. Jordan I. Teitelbaum and Dane M. Barrett.(2020).Nasal Airway Obstruction Structure and Function.JAMA Otolaryngology–Head & Neck Surgery(5),512–512.
5. Jean Bousquet,Ludger Klimek,Hans Christian Kuhl,Duc Tung Nguyen,Rajesh Kumar Ramalingam,G Walter Canonica,William Berger.Double-blind, placebo-controlled trial of the efficacy and safety of azelastine hydrochloride in children with perennial allergic rhinitis.[J].International archives of allergy and immunology,2024,11–15.
6. K. Gowthame,S. Prabakaran,R. B. Namasivaya Navin,S. Rajasekaran,R. Muthukumar,D. Balaji,B. Sarath Kumar,R. Lakshana.Prevalence of Fungal Sinusitis in Cases of Allergic Rhinitis: A Cross-Sectional Study[J].Indian Journal of Otolaryngology and Head & Neck Surgery,2024,(prepublish):1–4.
7. Xi Zhang,Min Yan,Qicheng Deng,Ling Yang.The efficacy and safety of radiofrequency ablation for allergic rhinitis: a systematic review and meta-analysis.[J].The Journal of laryngology and otology,2024,11–10.
8. Yiwei Hua,Xi Tan,Jingwen Zhang,Ningcong Xu,Ruien Chen,Shiqing Zhou,Shaoqing Liu,Kai Li,Wenyong Chen,Qiulan Luo,Yunying Li.Deciphering the pharmacological mechanism of Radix astragali for allergic rhinitis through network pharmacology and experimental validation[J].Scientific Reports,2024,14(1):29873–29873.
9. Feng Wen Shan,Min Zhou,Xin Yi Zheng,Tong Wu,Ya Na Zhang,Shuo Wu,Zhao Hui Shi,Xin Luo,Gui Xian Liang,He Zhang,He Xiao Jiang,Ning Kang,Yu Lian Chen,Qi Lin Zhou,Guo Wei Xiong,Jing Su,Yun Cheng,Xue Kun Huang,Guang Hui Dong,Qin Tai Yang.Risk Factors for Severe Allergic Rhinitis and the Association with Serum sIgE Levels: A Study in Guangzhou, China.[J].International archives of allergy and immunology,2024,11–18.

10. Fatema Mollah,Harvey L Leo.Long-Term Efficacy of House Dust Mite Sublingual Immunotherapy on Clinical and Pulmonary Function in Patients With Asthma and Allergic Rhinitis.[J].Pediatrics,2024,154(Suppl 4):S19.
11. Priscilla Campos,Solange O R Valle,Antônio José Ledo Alves da Cunha,Fábio Chigres Kuschnir,Dirceu Solé.Validation and reproducibility of the International Study of Asthma and Allergies in Childhood (ISAAC) Written Allergic Rhinitis Questionnaire for phone survey in children aged 6–7 years.[J].Brazilian journal of otorhinolaryngology,2024,91(2):101531.
12. Ayumi Shimamura,Hiroki Ishii,Tomokazu Matsuoka,Daisuke Watanabe,Takaaki Yonaga,Keisuke Masuyama,Daiju Sakurai.Prevalence Survey on Oral Allergy Syndrome in Patients With Seasonal Allergic Rhinitis in Yamanashi, Japan.[J].Allergy,2024,
13. Yingjie Yu,Xiaohui Yan,Lixin Wang,Lun Dong,Dong Song,Jing Liu,Xiaoping Gao.Investigation and Analysis of Inhalant Allergens in Patients with Allergic Rhinitis in Yinchuan, China.[J].International archives of allergy and immunology,2024,1–9.
14. Mehdi Torabizadeh,Mojtaba Aghaei,Najmaldin Saki,Mohammad A Vahid,Saeid Bitaraf,Bita Bandar.The Association of Nasal and Blood Eosinophils with Serum IgE Level in Allergic Rhinitis and Asthma: A Case-Control Study.[J].Health science reports,2024,7(11):e70191.
15. Chang Keun Kim,Yoonha Hwang,Dae Jin Song,Jinho Yu,Myung Hyun Sohn,Yong Mean Park,Dae Hyun Lim,Kangmo Ahn,Yeong Ho Rha.Efficacy and Safety of Montelukast+Levocetirizine Combination Therapy Compared to Montelukast Monotherapy for Allergic Rhinitis in Children.[J].Allergy, asthma & immunology research,2024,16(6):652–667.
16. Cuiqing Bai,Nan Zhang,Han Li,Yan Sun,Yinglan Wang,Chunxiang Zhou,Zhitong Zuo.Radioactive X-ray image examination in the treatment of allergic rhinitis asthma syndrome with traditional Chinese medicine[J].Journal of Radiation Research and Applied Sciences,2024,17(4):101149–101149.
17. Kenshiro Tabata,Yukiyoshi Sumi,Hatoko Sasaki,Noriko Kojimahara.Effectiveness of Intranasal Corticosteroids for Sleep Disturbances in Patients with Allergic Rhinitis: A Systematic Review and Meta-Analysis.[J].International archives of allergy and immunology,2024,11–15.
18. Zhao Zhang,Khawar Ali Shahzad,Xuran Li,Boyu Cai,Maoxiang Xu,Jiaojiao Li,Fei Tan.Immunomodulatory effect of mesenchymal stem cells-derived extracellular vesicles to modulate the regulatory T cells and Th1/Th2 imbalance in peripheral blood mononuclear cells of patients with allergic rhinitis.[J].Scandinavian journal of immunology,2024,100(6):e13416.
19. Andrea Ciofalo,Antonella Loperfido,Carlo Cavaliere,Maria Nicastri,Elona Begvarfaj,Francesca Cascone,Gianluca Bellocchi,Simonetta Masieri,Giovanni Ruoppolo.Allergic Rhinitis in Professional Singers: A Monoinstitutional Series.[J].Journal of voice : official journal of the Voice Foundation,2024,
20. Jiayan Wang,Bohuai Xu,Xujin Jia,Yong He,Beibei Jia,Junyuan Li,Ming Xu.Predictive value of Der p 2-specific IgE for subcutaneous immunotherapy in children with allergic rhinitis[J].Scientific Reports,2024,14(1):25467–25467.
21. Lauren M. Cook,Grace A. Longfellow,Julia C. Kessel,Brian D. Thorp,Adam J. Kimple,Cristine N. Klatt Cromwell,Brent A. Senior,Charles S. Ebert.Direct Comparison of Quality of Life in Patients with Allergic Rhinitis Undergoing Sublingual Versus Subcutaneous Immunotherapy[J].Journal of Clinical Medicine,2024,13(21):6397–6397.
22. Catarina Isabel Medalhas Rebelo da Silva,Rosa Martins,Rosário Ferreira.Impact of asthma and allergic rhinitis control on sleep disordered breathing in pediatrics[J].Sleep Medicine: X,2024,8100129–100129.
23. Marn Joon Park, Mirye Bae, Ji Heui Kim, Yoo Sam Chung,Yong Ju Jang and Myeong Sang Yu.(2024).Impact of long-term nasal airflow deprivation on sinonasal structures and chronic rhinosinusitis in total laryngectomy patients..Laryngoscope investigative otolaryngology(1),e1214–e1214.
24. Cui Pengbo,Li Mengyu,Shao Tianlun,Yu Mingxiao,Zhao Weixue,Song Yanzhuo... and Liu Jianhua.(2023).Preparation, structure characterization, and stability analysis of peptide-calcium complex derived from porcine nasal cartilage type II collagen..Journal of the science of food and agriculture(14),6884–6894.
25. Oshita Ryo, Katayose Sakie,Kanai Eiichi and Takagi Satoshi.(2022).Assessment of Nasal Structure Using CT Imaging of Brachycephalic Dog Breeds.Animals(13),1636–1636.
26. Lou Miao,Zhang Luyao,Zhang Jingbin,Ma Ruiping,Gong Minjie,Hu Zhenzhen... and Zheng Guoxi.(2021).Numerical Simulation of Nasal Airflow Aerodynamics, and Warming and Humidification in Models of Clival Chordoma Pre and Post-Endoscopic Endonasal Surgery..Respiratory physiology & neurobiology103693–103693.
27. Zeng Minjie and Zhu Guochen.(2021).Nasal Septal Swell Body: A Distinctive Structure in the Nasal Cavity..Ear, nose, & throat journal1455613211010093–1455613211010093.

28. Shorook N ,Boris K ,Ziv G , et al.Endoscopic Septoplasty Versus Traditional Septoplasty for Treating Deviated Nasal Septum: A Prospective, Randomized Controlled Trial.[J].Ear, nose, & throat journal,2020,100(9):145561320918982.